Mineralogical Magazine (2020), **84**, 859–868
doi:10.1180/mgm.2020.79

CAMBRIDGE UNIVERSITY PRESS

Article

Sulfide partial melting and galena–tetrahedrite intergrowth texture: An experimental study

Boddepalli Govindarao, Kamal Lochan Pruseth* and Biswajit Mishra
Department of Geology and Geophysics, Indian Institute of Technology, Kharagpur 721302, India

Abstract

Galena–tetrahedrite intergrowth textures have been observed in some quenched run products of melting experiments conducted at 500 and 600°C in the systems ZnS–PbS–FeS–Cu_2S–Sb_2S_3 and ZnS–PbS–FeS–Cu_2S–Sb_2S_3–As_2S_3, using the evacuated silica-tube method. At 600°C the intergrowth formed an interface between sulfide melt and galena, whereas at 500°C it existed as inclusions partially embedded or completely embedded within tetrahedrite. At 600°C tetrahedrite was absent in PbS-bearing experiments, instead galena and melt were a part of the equilibrium phase assemblage. From the disposition of the galena–tetrahedrite intergrowths at 500°C it is evident that droplets of galena–tetrahedrite melt coexisted with tetrahedrite or tetrahedrite + galena and gave rise to these intergrowths upon quenching. The intergrowths coexisting with galena probably represent compositions on the galena-rich liquidus in the galena–tetrahedrite binary and those coexisting with tetrahedrite represent points on the tetrahedrite-rich liquidus. A eutectic at galena:tetrahedrite = ~30:70, very close to 500°C is apparent. It is clearly indicated that galena–tetrahedrite intergrowths can be formed by sulfide partial melting, and could be used as a potential indicator of partial melting in metamorphosed sulfide ore deposits.

Keywords: partial melting, eutectic, co-crystallisation, co-precipitation, replacement

(Received 6 July 2020; accepted 16 October 2020; Accepted Manuscript published online: 20 October 2020; Associate Editor: Makoto Arima)

Introduction

Intergrowth textures of sulfide minerals have been observed extensively: e.g. bornite–chalcocite (Schwartz, 1939; Ramdohr, 1969; Cook *et al.*, 2011), bornite–galena (Kouzmanov, 2004), sphalerite–chalcopyrite (Govindarao *et al.*, 2018 and references therein), galena–stromeyerite (Schwartz and Park, 1932; Ramdohr, 1969), galena–cosalite (Anderson, 1934; Ramdohr, 1969) and galena–pyrargyrite (Anderson, 1934; Ramdohr, 1969). Symplectitic or myrmekitic intergrowth of galena and tetrahedrite (Fig. 1) has been also observed in many sulfide ore deposits (Lindgren, 1930; Anderson, 1934; Basu *et al.*, 1984; Gemmell *et al.*, 1989; Cook, 1996; Cook *et al.*, 1998; Brueckner *et al.*, 2016). Ramdohr (1969) suggested more than six mechanisms for the formation of such intergrowths. For the formation of galena–tetrahedrite intergrowths, hydrothermal replacement (Lindgren, 1930; Anderson, 1934) and co-precipitation (Gemmell *et al.*, 1989) are the mechanisms most favoured. In contrast, galena–tetrahedrite intergrowths at Sulitjelma and Bleikvassli hydrothermal ore deposits, Norway, were interpreted as formed by the breakdown of meneghinite to galena and tetrahedrite in the presence of a Cu–Fe–(Ag) fluid (Cook, 1996; Cook *et al.*, 1998). Ambiguity arises in interpreting these intergrowth textures, especially when encountered in metamorphosed sulfide ore deposits in which metamorphic recrystallisation obliterates primary textural features. Galena and tetrahedrite from Rajpura-Dariba hydrothermal ore deposit, India have intergrowth textures, which were surmised to have formed through the breakdown of complex sulfosalt minerals or through oriented mineral growth from hydrothermal solution or sulfide melt (Basu *et al.*, 1984). Note that Pruseth *et al.* (2014, 2016) decscribed evidence of sulfide melting and melt fractionation during amphibolite-facies metamorphism of the Rajpura-Dariba polymetallic sulfide ores. Frost *et al.* (2002) also proposed the partial melting of the Sulitjelma and Bleikvassli sulfide ore deposits during medium- and high-grade metamorphism. In view of the growing acceptance of sulfide anatexis as a viable geological process (Mavrogenes *et al.*, 2001; Frost *et al.*, 2002, 2005, 2011; Tomkins and Mavrogenes, 2002, 2003; Sparks and Mavrogenes, 2005; Tomkins *et al.*, 2007; Mishra and Bernhardt, 2009; Pruseth *et al.*, 2014, 2016; Govinda Rao *et al.*, 2017; Matt *et al.*, 2019) it is necessary to evaluate if sulfide partial melting could be responsible for the formation of these intergrowths. This work describes the results of experiments in the system ZnS–PbS–FeS–Cu_2S–Sb_2S_3 and ZnS–PbS–FeS–Cu_2S–Sb_2S_3–As_2S_3, conducted at 500 and 600°C using the evacuated silica-tube method.

Experimental and analytical methods

All experiments were conducted using the evacuated silica tube method as described by Scott (1974) and Pruseth *et al.* (1997). High-purity (>99% SiO_2) silica tubes of 6 mm internal diameter and 1 mm wall thickness were used. Generally, the evacuated silica ampules had a length of ~2 cm, with the charge confined to ~0.5 cm at one end, the rest being occupied by a snugly fitting filler rod of the same material as the silica tube. Samples were

*Author for correspondence: Kamal Lochan Pruseth, Email: pruseth@gg.iitkgp.ac.in
Cite this article: Govindarao B., Pruseth K.L. and Mishra B. (2020) Sulfide partial melting and galena–tetrahedrite intergrowth texture: An experimental study. *Mineralogical Magazine* **84**, 859–868. https://doi.org/10.1180/mgm.2020.79

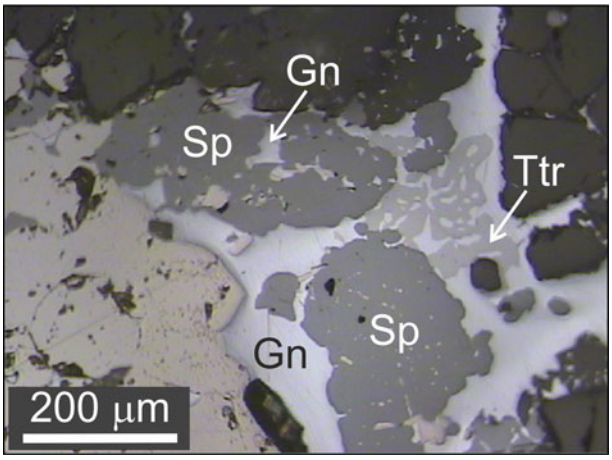

Fig. 1. Microphotograph of a typical tetrahedrite–galena intergrowth texture. Sample from Rajpura-Dariba, Rajasthan, India.

heated in a Lenton (UK) box furnace with inbuilt EUROTHERM temperature controllers, and the temperature in the hot zone of the furnace was externally monitored by a Pt–$Pt_{90}Rh_{10}$ thermocouple. The temperature in the hot zone of the furnace was maintained within ±2°C of the set temperature. High-purity elemental Zn, Fe, Pb, Cu, Sb and S from Alfa Aesar (Thermo Fisher Scientific, UK) were used for the synthesis of ZnS, FeS, PbS, Cu_2S and Sb_2S_3 end-member phases. Zinc ingots were abraded to a fine powder and reacted with sulfur at 400°C for 2 days and at 500°C for 5 days for synthesising the ZnS phase. Compared to Zn metal, ZnS is extremely refractory, with a melting temperature of 1680°C (Mavrogenes *et al.*, 2001). Therefore, if Zn ingots are used directly, ZnS formed at the surface prevents the Zn at the core of the individual ingots from further reaction. The use of fine filings of zinc helps circumvent this problem. The PbS phase was prepared from pieces of pure Pb metal, cut from a sheet after removing the thin oxidised coating, by reaction with sulfur at 500°C for 8 days. For the synthesis of the FeS phase, iron powder was reduced in a hydrogen flow at 750°C for 4 hours then heated with stoichiometric proportions of sulfur at 400°C for 4 days and further at 600°C for 5 days. For the synthesis of the Cu_2S phase, a copper rod was abraded to fine grains, which were briefly cleaned with dilute HCl and washed with distilled water. These copper filings were reacted with sulfur initially at 200°C for 2 days and finally at 400°C for 9 days. Both the FeS and Cu_2S phases are non-stoichiometric and have cation deficiencies. Thus, to obtain stoichiometric FeS and Cu_2S phases, a few larger pieces of Fe and Cu were reacted with the respective finely powdered synthesis products as a final step. The unreacted remnant pieces were removed by gently grinding the final synthesis products under acetone and picking the resistant grains out. Pure Sb metal was reacted with sulfur at 500°C for 8 days for the synthesis of the Sb_2S_3 phase. The successful synthesis of the end-members was ascertained by matching the X-ray diffraction patterns of these phases with the corresponding patterns in the ICDD reference data base [www.icdd.com/]. The pure crystalline As_2S_3 phase procured from Alfa Aesar was used directly in the experiments. Experiments were conducted at 500 and 600°C with accurately weighed different amounts of ZnS, PbS and FeS with 5 mol.% of Cu_2S and either 5 or 10 mol.% Sb_2S_3 in the system ZnS–PbS–FeS–Cu_2S–Sb_2S_3. In the system ZnS–PbS–FeS–Cu_2S–Sb_2S_3–As_2S_3, the proportions of ZnS, PbS and FeS together comprise 90 mol.% of the bulk; 5 mol.% of Cu_2S; and 2.5 mol.% each of Sb_2S_3 and As_2S_3 make up the rest. The starting bulk compositions were chosen in order to check the effect of incorporating Sb_2S_3 and As_2S_3, in addition to Cu_2S, on melting in the system ZnS–PbS–FeS. The ternary eutectic in the pure ZnS–PbS–FeS system is determined at 800°C (Mavrogenes *et al.*, 2001), though the incorporation of Cu_2S results in the reduction of the melting temperature and a quaternary eutectic has been reported at ~593°C (Pruseth *et al.*, 2014). One run was conducted with 5 mol.% each of Cu_2S and Sb_2S_3 on the ZnS–FeS binary of the ZnS–PbS–FeS system to check the nature of melting in the absence of PbS.

The run products, mounted in cold-setting epoxy, were ground, polished and analysed with a CAMECA SX100 electron probe micro-analyser (EPMA) and back-scattered electron (BSE) images were obtained with a JEOL JSM6490 scanning electron microscope (SEM) at the Department of Geology and Geophysics, IIT, Kharagpur, India. The typical operating conditions on the EPMA were 20 kV accelerating voltage, 20 nA beam current and 1 µm beam diameter. The quenching of melt produced by partial melting of the starting materials was not successful because of the crystallisation of quench crystals, hence the average composition of the quenched melt in each run, measured using a rather large beam diameter (20 µm) under similar conditions, was assumed to be the closest possible representative composition of the quenched melt. The X-ray lines used for the analysis of S, Fe, Cu, Zn, As, Sb and Pb are S*Kα*, Fe*Kα*, Cu*Kα*, Zn*Kα*, As*Lα*, Sb*Lα* and Pb*Mα*, respectively. Natural and synthetic standards used for calibration were: pyrite for Fe and S; sphalerite for Zn; galena for Pb; GaAs for As; stibnite for Sb; and pure Cu metal for Cu. All the standards were from P&H Developments Ltd. (UK). All elements were analysed for ten seconds on the peak and five seconds each on either side of the peak. The ZAF corrections were made by the program available with the CAMECA SX-100 operating software. Counting errors were limited to 0.01%.

Results

The bulk compositions of all the experimental runs, the respective durations of the experiments and the EPMA of the equilibrium phases obtained in the system ZnS–PbS–FeS–Cu_2S–Sb_2S_3 and ZnS–PbS–FeS–Cu_2S–Sb_2S_3–As_2S_3 are given in Table 1 and Table 2, respectively. All mineral abbreviations in the tables and figures are after Whitney and Evans (2010).

The system ZnS–PbS–FeS–Cu_2S–Sb_2S_3

Three experimental runs (G3, G4 and G9) conducted at 600°C contain 5 mol.% each of Cu_2S and Sb_2S_3, with varying proportions of PbS, FeS and ZnS in two runs (G3 and G4) and with 50 mol.% ZnS and 40 mol.% FeS in one run (G9). Significant melting occurred in runs G3 and G4, whereas only a small amount of melt, which could not be analysed, is observed in the PbS-free run G9. The melt compositions together with the corresponding bulk compositions are plotted in Figs 2a and 2b, and the representative SEM-BSE images of stable run products are shown in Figs 3a–c. The melt composition in the respective run products is the average of EPMA of several areas obtained using a defocused beam of 20 µm. The resultant sulfide melts are enriched in Pb (37.07–38.11 wt.%), Cu (18.67–25.37 wt.%) and Sb (17.28–20.06 wt.%) relative to Fe (0.82–3.43 wt.%) and

https://doi.org/10.1180/mgm.2020.79 Published online by Cambridge University Press

Table 1. Details of the run compositions from EPMA of different phases obtained in the system ZnS–PbS–FeS–Cu_2S–Sb_2S_3*.

Run	Mol %					Duration (Days)	Weight %						Total	Formula						Phase (*n*)
	PbS	FeS	ZnS	Cu_2S	Sb_2S_3		S	Fe	Cu	Zn	Sb	Pb		S	Fe	Cu	Zn	Sb	Pb	
600°C																				
G3	49.5	13.5	27.0	5.0	5.0	8	35.10 (0.18)	15.77 (0.13)	0.35 (0.06)	49.65 (0.09)	n.d.	n.d.	100.86	1	0.26	0.00	0.69			Sp (8)
							13.96 (0.13)	0.02 (0.03)	0.28 (0.06)	0.10 (0.12)	0.79 (0.05)	86.00 (0.86)	101.15	1	0.00	0.01	0.00	0.01	0.95	Gn (8)
							20.70 (0.14)	3.43 (0.23)	18.67 (1.83)	0.33 (0.12)	20.06 (0.87)	38.11 (1.05)	101.31	1	0.10	0.46	0.01	0.26	0.28	Melt (9)
G4	23.0	5.0	63.0	5.0	5.0	8	33.87 (0.37)	3.33 (0.08)	0.28 (0.14)	63.45 (0.56)	n.d.	n.d.	100.92	1	0.06	0.00	0.92			Sp (12)
							14.14 (0.09)	n.d.	0.52 (0.08)	0.51 (0.32)	0.64 (0.06)	85.98 (0.82)	101.79	1		0.02	0.02	0.01	0.94	Gn (10)
							19.76 (0.40)	0.82 (0.11)	25.37 (1.34)	0.73 (0.18)	17.28 (0.40)	37.07 (0.50)	101.02	1	0.02	0.65	0.02	0.23	0.29	Melt 1 (8)
G9	0.0	40.0	50.0	5.0	5.0	10	35.22 (0.24)	24.50 (0.23)	1.73 (0.07)	39.96 (0.49)	n.d.		101.40	1	0.40	0.02	0.56		0.00	Sp (7)
							35.96 (0.13)	41.63 (0.11)	15.45 (0.35)	8.28 (0.28)	n.d.		101.32	3	1.99	0.65	0.34		0.00	Cbn (6)
							25.68 (0.27)	5.91 (0.38)	35.40 (0.41)	3.28 (0.30)	30.14 (0.43)		100.41	13	1.72	9.04	0.81	4.02	0.00	Ttr (10)
500°C																				
G10	49.5	13.5	27.0	5.0	5.0	17	34.58 (0.37)	15.83 (0.84)	0.49 (0.28)	48.65 (0.91)	n.d.	n.d.	99.55	1	0.26	0.01	0.69			Sp (9)
							13.80 (0.35)	n.d.	0.21 (0.13)	0.36 (0.29)	0.25 (0.09)	86.59 (0.73)	101.21	1		0.01	0.01	0.00	0.97	Gn (7)
							25.34 (0.28)	4.82 (0.32)	37.36 (0.63)	3.33 (0.79)	29.44 (0.56)	n.d.	100.28	13	1.42	9.67	0.84	3.98		Ttr (7)
G11	40.0	38.0	12.0	5.0	5.0	17	34.90 (0.23)	22.26 (0.64)	0.59 (0.01)	41.62 (0.67)	n.d.	n.d.	99.36	1	0.37	0.01	0.58			Sp (4)
							13.85 (0.11)	0.23 (0.06)	0.17 (0.08)	0.18 (0.13)	0.71 (0.08)	85.96 (0.42)	101.11	1	0.01	0.01	0.01	0.01	0.96	Gn (8)
							35.57 (0.63)	43.14 (0.70)	16.77 (0.29)	4.36 (0.12)	n.d.	n.d.	99.84	3	2.09	0.71	0.18			Cbn (8)
							17.66 (0.34)	0.38 (0.12)	2.05 (0.13)	0.20 (0.11)	18.61 (0.46)	61.47 (0.96)	100.37	24	0.30	1.41	0.13	6.66	12.93	Mgt (6)
G12	38.0	36.0	11.0	5.0	10.0	18	34.63 (0.80)	20.46 (1.67)	0.51 (0.18)	44.30 (0.53)	n.d.	n.d.	99.91	1	0.34	0.01	0.63			Sp (5)
							13.49 (0.16)	0.16 (0.08)	0.16 (0.09)	0.12 (0.05)	0.74 (0.05)	85.25 (0.97)	99.93	1	0.01	0.01	0.00	0.01	0.98	Gn (7)
							34.95 (0.36)	42.80 (0.56)	17.12 (0.15)	4.53 (0.21)	n.d.	n.d.	99.40	3	2.11	0.74	0.19			Cbn (12)
							17.57 (0.31)	0.24 (0.10)	2.09 (0.10)	0.26 (0.19)	18.57 (0.30)	61.93 (0.80)	100.66	24	0.19	1.44	0.17	6.68	13.09	Mgt (12)

'n.d.' stands for not detected. Melt compositions were obtained using a defocussed beam of 20 μm in diameter. Abbreviations: Cbn-cubanite, Gn-galena, Mgt-meneghinite, Po-pyrrhotite, Sp-sphalerite, Ttr-tetrahedrite

*The compositions of the phases are averages of the number of analyses (*n*) indicated and the respective standard deviations are given in parentheses

Zn (0.33–0.73 wt.%). The melts are S deficient over the total wt.% of metals (Σmetals) (Table 1). The other stable phases present are: galena, sphalerite and native Sb in G3 and G4; and sphalerite, Zn-bearing cubanite (containing 3.31–8.28 wt.% Zn), tetrahedrite and native Sb in G9. A phase similar to Zn-bearing cubanite was obtained in a previous investigation and was referred to as an ISS (intermediate solid solution) of cubanite ($CuFe_2S_3$) composition containing significant Zn (Kojima and Sugaki, 1984). We have referred to this phase as cubanite, as irrespective of differences in composition, the total cation number tends to equal three when normalised to three S atoms. Note, however, that this phase might be equivalent to Zn-bearing isocubanite, as cubanite changes irreversibly from hexagonal to cubic symmetry at 210°C (Cabri *et al.*, 1973; Putnis, 1977). However, in the absence of structural details, we have called it simply 'cubanite'. Although Zn replaces Fe in Zn-bearing cubanite, and it sounds more natural considering the disordered sphalerite-like structure of isocubanite (Fleet, 1970; Szymanski, 1974), a strong negative correlation between the Cu and Zn in it is evident. The absence of any evidence of disequilibrium, such as compositional zonation in the solid phases and intra-grain and inter-grain homogeneity of the run products, as evident from numerous EPM spot analyses, indicate attainment of chemical equilibrium. Reproducibility of results in experiments involving similar bulk compositions, although of different duration of heating, further indicate attainment of equilibrium. In G3 and G4, tiny galena grains, seen rimming the sphalerite (e.g. Figs 3a and 3b), contain up to 0.7–2.2 wt.% Zn, 1.2–2.8 wt.% Cu, 0.8–1.7 wt.% Sb and 0.1–0.7 wt.% Fe. As shown in Fig. 3b, the presence of two melts in G4 is evident. Melt 1 crystallised to a fine-grained assemblage and has a composition similar to tetrahedrite with excess Pb. Melt 2 crystallised to an intergrowth of coarse-grained galena with composition $Pb_{0.93}Cu_{0.08}Zn_{0.06}Sb_{0.02}S$ and tetrahedrite of composition $Cu_6[Cu_{3.66}(Fe_{0.67}Zn_{0.51}Pb_{0.77})_{\Sigma 1.95}]Sb_{4.03}S_{12}S$ (Fig. 3b). The formula for tetrahedrite is after Biagioni *et al.* (2020), who suggest the structural formula $A_6(B_4C_2)D_4Y_{12}Z$, in which the sites *A*

https://doi.org/10.1180/mgm.2020.79 Published online by Cambridge University Press

Table 2. Details of the run compositions from EPMA of different phases obtained in the system ZnS–PbS–FeS–Cu_2S–Sb_2S_3–As_2S_3.

	Mol %							Weight %								Formula							
	PbS	FeS	ZnS	Cu_2S	Sb_2S_3	As_2S_3	Duration (days)	S	Fe	Cu	Zn	As	Sb	Pb	Total	S	Fe	Cu	Zn	As	Sb	Pb	Phase (*n*)
600°C																							
G51	13.5	49.5	27.0	5.0	2.5	2.5	10	34.53 (0.29)	21.27 (0.38)	1.40 (0.12)	42.78 (0.48)	n.d.	n.d.	n.d.	99.98	1	0.35	0.02	0.61				Sp (12)
								13.75 (0.18)	0.12 (0.07)	0.12 (0.06)	0.23 (0.13)	0.01 (0.01)	0.84 (0.09)	85.56 (0.73)	100.64	1	0.01	0.00	0.01	0.00	0.02	0.96	Gn (7)
								38.55 (0.18)	58.95 (0.24)	1.96 (0.21)	0.17 (0.18)	n.d.	n.d.	n.d.	99.63	1	0.88	0.03	0.00				Po (5)
								35.87 (0.36)	40.16 (0.38)	16.60 (0.28)	7.62 (0.21)	n.d.	n.d.	n.d.	100.25	3	1.93	0.70	0.31				Cbn (9)
								20.65 (0.57)	5.03 (0.65)	7.66 (0.47)	0.53 (0.15)	10.08 (1.38)	17.04 (0.89)	40.90 (1.04)	101.89	1	0.14	0.19	0.01	0.21	0.22	0.31	Melt (8)
G52	10.4	15.8	63.9	5.0	2.5	2.5	10	33.30 (0.27)	9.88 (0.18)	0.44 (0.11)	55.74 (0.21)	n.d.	n.d.	n.d.	99.35	1	0.17	0.01	0.82				Sp (7)
								14.24 (0.34)	0.37 (0.10)	1.54 (0.18)	1.14 (0.33)	0.28 (0.13)	1.91 (0.23)	81.65 (0.96)	101.14	1	0.02	0.05	0.04	0.01	0.04	0.89	Gn (5)
								21.00 (0.30)	2.14 (0.25)	13.23 (0.67)	1.00 (0.63)	8.45 (0.65)	12.83 (0.71)	41.33 (0.53)	99.98	1	0.06	0.32	0.02	0.17	0.16	0.30	Melt (9)
G53	49.5	13.5	27.0	5.0	2.5	2.5	10	33.95 (0.25)	14.04 (0.22)	0.88 (0.07)	50.54 (0.25)	n.d.	n.d.	n.d.	99.40	1	0.24	0.01	0.73				Sp (15)
								13.66 (0.21)	0.03 (0.04)	0.16 (0.07)	0.12 (0.15)	0.01 (0.01)	0.54 (0.05)	85.57 (0.75)	100.07	1	0.00	0.01	0.00	0.00	0.01	0.97	Gn (12)
								35.39 (0.31)	36.98 (0.40)	20.77 (0.16)	6.29 (0.10)	n.d.	n.d.	n.d.	99.42	3	1.80	0.89	0.26				Cbn (4)
								21.02 (0.49)	2.84 (0.65)	12.54 (1.40)	1.05 (0.74)	7.75 (1.27)	12.27 (1.54)	42.76 (1.41)	100.23	1	0.08	0.30	0.02	0.16	0.15	0.31	Melt (7)
G54	22.5	4.5	63.0	5.0	2.5	2.5	10	33.39 (0.41)	3.24 (0.09)	0.22 (0.06)	62.76 (0.52)	n.d.	n.d.	n.d.	99.61	1	0.06	0.00	0.92				Sp (11)
								13.80 (0.12)	n.d.	0.24 (0.09)	0.30 (0.22)	n.d.	0.63 (0.08)	85.99 (0.69)	100.97	1		0.01	0.01		0.01	0.96	Gn (8)
								20.09 (1.04)	0.86 (0.14)	13.62 (1.05)	2.01 (0.49)	8.54 (0.59)	12.16 (0.93)	42.43 (1.53)	99.71	1	0.02	0.34	0.05	0.18	0.16	0.33	Melt (6)
500°C																							
G55	13.5	49.5	27.0	5.0	2.5	2.5	27	34.33 (0.59)	15.02 (0.57)	0.40 (0.07)	51.19 (0.79)	n.d.	n.d.	n.d.	100.94	1	0.25	0.01	0.73				Sp (10)
								13.33 (0.10)	0.31 (0.07)	0.14 (0.12)	0.53 (0.16)	n.d.	0.76 (0.05)	85.88 (0.78)	100.96	1	0.01	0.01	0.02		0.01	1.00	Gn (4)
								34.45 (0.90)	40.69 (0.27)	19.92 (0.60)	3.95 (0.17)	n.d.	n.d.	n.d.	99.01	3	2.05	0.88	0.17				Cbn (11)
								17.43 (0.19)	0.78 (0.17)	1.51 (0.13)	0.95 (0.34)	1.47 (0.07)	17.62 (0.33)	61.22 (0.45)	100.97	24	0.73	1.08	0.69	0.85	6.35	12.95	Mgt (6)

https://doi.org/10.1180/mgm.2020.79 Published online by Cambridge University Press

G56	10.4	15.8	63.9	5.0	2.5	2.5	27		33.62 (0.39)	9.28 (0.30)	0.10 (0.16)	57.46 (0.67)	n.d.	n.d.	n.d.	100.45	1	0.16	0.00	0.84				Sp (12)
									33.91 (0.48)	36.79 (0.78)	24.52 (0.43)	3.77 (0.21)	0.25 (0.08)	n.d.	n.d.	99.25	3	1.87	1.09	0.16	0.01			Cbn (8)
									26.35 (0.32)	5.49 (0.54)	39.96 (0.87)	4.08 (0.60)	10.91 (0.81)	14.37 (0.67)	n.d.	101.14	13	1.55	9.95	0.99	2.30	1.87		Ttr–Tnt_{ss} (9)
									16.91 (0.26)	0.13 (0.12)	0.08 (0.08)	1.45 (1.19)	4.47 (0.26)	9.80 (0.29)	67.90 (1.18)	100.74	23	0.10	0.06	0.96	2.60	3.51	14.29	Geo (7)
G57	49.5	13.5	27.0	5.0	2.5	2.5	27		33.67 (0.56)	9.30 (0.29)	0.27 (0.10)	56.42 (0.68)	n.d.	n.d.	n.d.	99.66	1	0.16	0.00	0.82				Sp (11)
									13.52 (0.26)	0.07 (0.10)	0.21 (0.15)	0.40 (0.24)	n.d.	0.59 (0.04)	85.87 (0.37)	100.66	1	0.00	0.01	0.01		0.01	0.98	Gn (9)
									34.52 (0.68)	37.15 (0.57)	23.68 (0.68)	3.31 (0.17)	0.68 (0.85)	n.d.	n.d.	99.33	3	1.85	1.04	0.14	0.03			Cbn (7)
									27.59 (0.31)	5.03 (0.18)	39.31 (0.66)	3.46 (0.14)	11.07 (0.51)	14.10 (0.24)	n.d.	100.61	13	1.36	9.35	0.80	2.23	1.75		Ttr–Tnt_{ss} (9)
									17.47 (0.29)	0.24 (0.23)	0.28 (0.24)	0.62 (0.53)	4.64 (0.23)	9.55 (0.37)	68.59 (0.67)	101.39	23	0.18	0.19	0.40	2.61	3.31	13.97	Geo (8)
G58	22.5	4.5	63.0	5.0	2.5	2.5	27		33.71 (0.43)	2.40 (0.49)	0.12 (0.10)	65.24 (1.02)	n.d.	n.d.	n.d.	101.24	1	0.04	0.00	0.95				Sp (12)
									13.63 (0.15)	0.01 (0.02)	0.32 (0.25)	0.37 (0.15)	0.01 (0.01)	0.63 (0.06)	85.78 (0.41)	100.75	1	0.00	0.00	0.01	0.01	0.01	0.97	Gn (8)
									35.08 (0.12)	37.36 (0.01)	24.07 (0.21)	3.40 (0.16)	0.21 (0.12)	n.d.	n.d.	100.11	3	1.83	1.04	0.14	0.01			Cbn (5)
									27.18 (0.36)	3.10 (0.41)	39.53 (0.58)	5.49 (0.71)	10.62 (0.40)	14.62 (0.28)	n.d.	100.64	13	0.87	9.54	1.27	2.17	1.84		Ttr–Tnt_{ss} (18)
									17.42 (0.16)	n.d.	0.38 (0.40)	0.86 (0.38)	4.49 (0.16)	9.85 (0.23)	67.67 (0.43)	100.65	23		0.25	0.56	2.54	3.43	13.83	Geo (10)

'n.d.' stands for not detected. Melt compositions were obtained using a defocussed beam of 20 μm in diameter. Abbreviations: Cbn – cubanite, Geo – geocronite, Gn – galena, Mgt – meneghinite, Po – pyrrhotite, Sp – sphalerite, Ttr–Tnt_{ss} – tetrahedrite–tennantinite solid solution

*The compositions of the phases are averages of the number of analyses (n) indicated and the respective standard deviations are given in parentheses

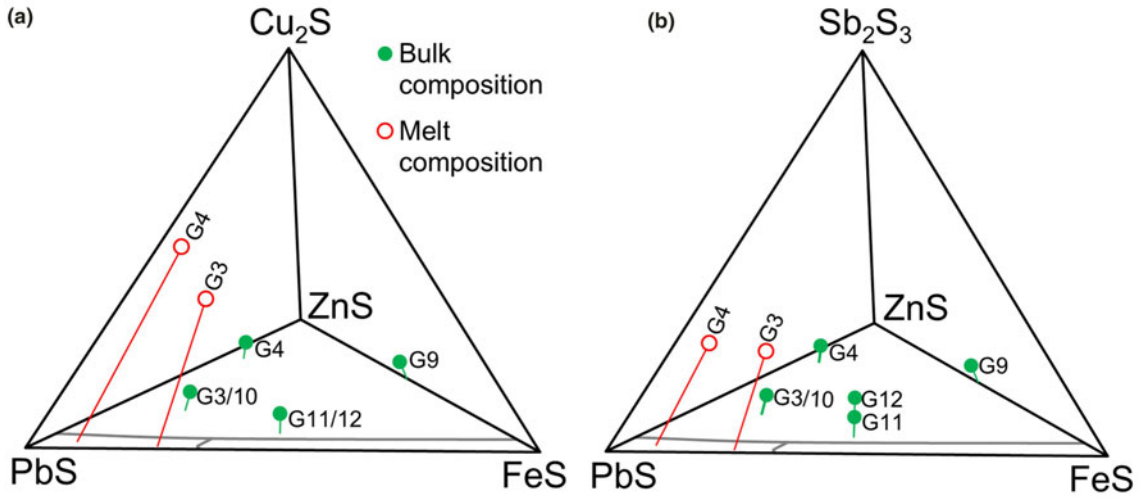

Fig. 2. Run and melt compositions of the experiments at 600°C (G3, G4 and G9) and 500°C (G10–G12) projected in the ZnS–PbS–FeS–Cu_2S (*a*) and ZnS–PbS–FeS–Sb_2S_3 (*b*) quaternary diagrams. Filled circles represent bulk compositions and the open circles represent corresponding melt compositions. The lengths of the sticks are proportional to the Cu_2S and Sb_2S_3 contents.

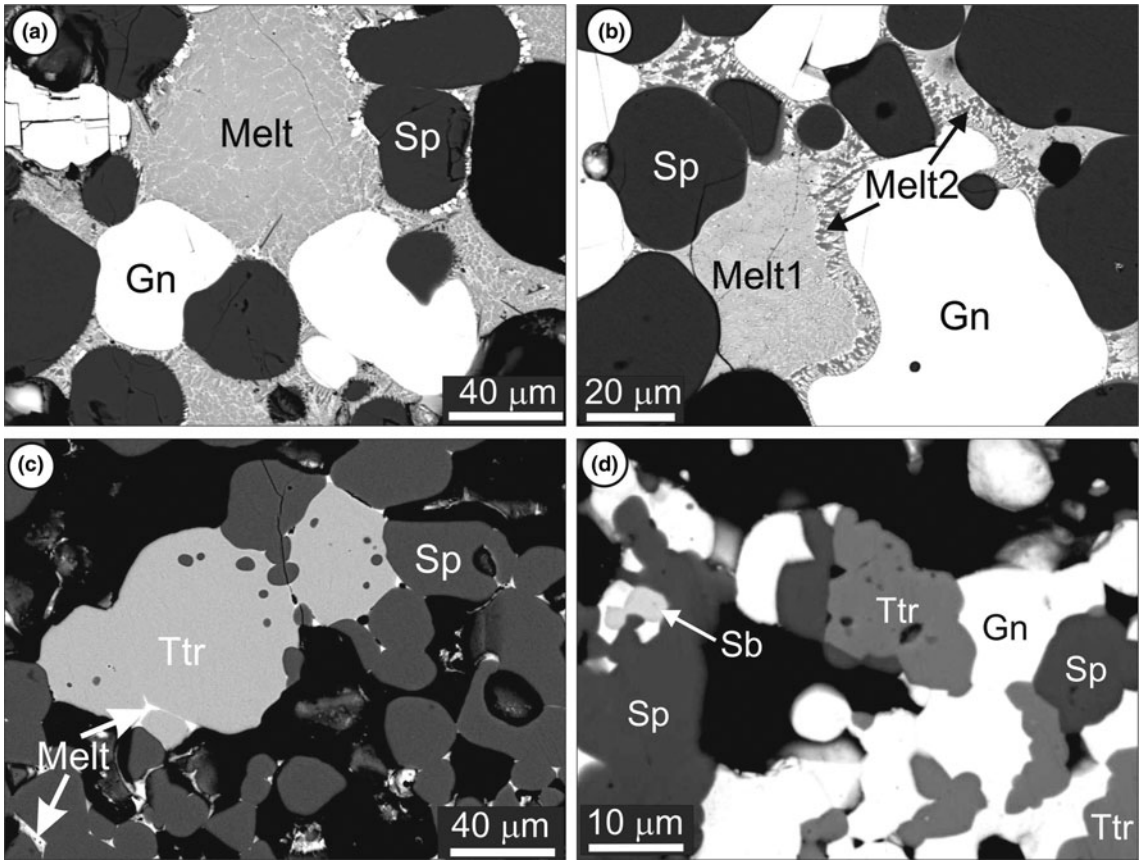

Fig. 3. BSE images showing stable phase assemblages in the runs G3, G4 and G9 (*a–c*, respectively) at 600°C and in the run G10 (*d*) at 500°C. Development of fine intergrowth of galena and tetrahedrite from melt 2 is seen in (*b*).

and *B* are occupied by Cu or Ag, C by Zn, Fe, Hg, Cd, Mn and Cu; *D* by Sb, As, Bi and Te; and *Y* and *Z* by S and Se. The presence of considerable Pb in the *C* site is a deviation from the suggested *C* site occupancy by cations such as Zn^{2+}, Fe^{2+}, Hg^{2+}, Cd^{2+}, Mn^{2+}, Cu^{2+}, Cu^{+} and Fe^{3+}. The incompatibility of Pb^{2+} arises from its relatively larger size (Biagioni *et al.*, 2020), however, rapid crystallisation from a melt in this case seems to have resulted in the incorporation of Pb. Similar incorporation of incompatible Zn

https://doi.org/10.1180/mgm.2020.79 Published online by Cambridge University Press

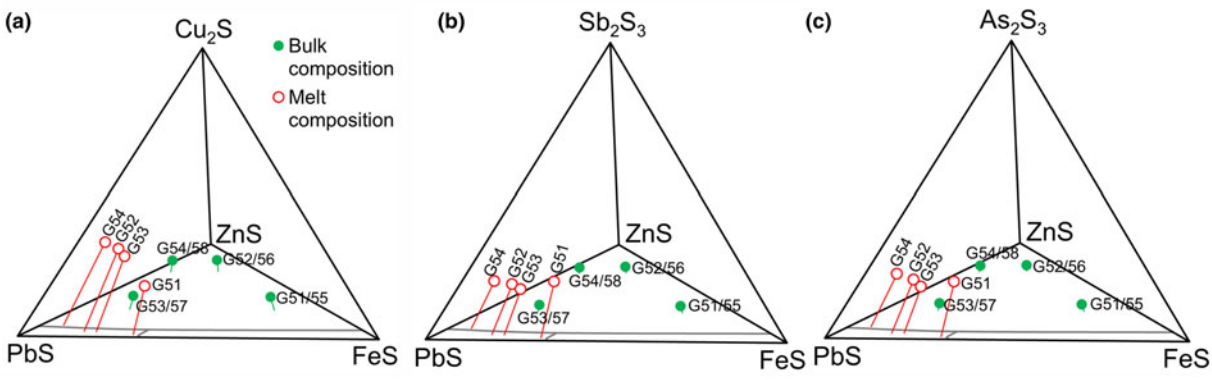

Fig. 4. Run and melt compositions of the experiments at 600°C (G51–G54) and 500°C (G55–G58) projected in the (*a*) ZnS–PbS–FeS–Cu_2S, (*b*), ZnS–PbS–FeS–Sb_2S_3 and (*c*) ZnS–PbS–FeS–Sb_2S_3 quaternary diagrams. Filled circles represent bulk compositions and the open circles represent melt compositions. The lengths of the sticks are proportional to the Cu_2S, Sb_2S_3 and As_2S_3 contents.

in galena, having formed from melt, is observed in this present investigation and has been also documented by Mavrogenes *et al.* (2013) in their experimental study.

The starting bulk composition of the three experimental runs (G10–G12) at 500°C are projected in Figs 2a and 2b. In G10, the bulk composition is similar to that of G3 at 600°C. No melt is encountered in any of the run products. Sphalerite and native Sb are common to all the run products. Although galena + tetrahedrite are stable in G10 (Fig. 3d), galena + Zn-bearing cubanite + meneghinite are stable in G11 and G12.

The system ZnS–PbS–FeS–Cu_2S–Sb_2S_3–As_2S_3

At 600°C, considerable melt is obtained in all four experiments (G51–G54). The composition of the melts together with the corresponding starting bulk compositions are projected in Figs 4a–c and are given in Table 2. In common with the experimental runs G3 and G4, the resultant melts are S-deficient over Σmetals and are richer in Pb (40.90–42.76 wt.%), Sb (12.16–17.04 wt.%), Cu (7.66–13.62 wt.%), As (7.75–10.08 wt.%) and relatively poorer in Fe (0.86–5.03 wt.%) and Zn (0.53–2.01 wt.%). Other than melt, sphalerite and galena are common to all the run products at 600°C. In addition, pyrrhotite + Zn-bearing cubanite are obtained in G51, and Zn-bearing cubanite in G54. As in the experimental runs G3 and G4, tiny crystals of galena appear in the quenched melt. Galena also forms rims along the boundary of sphalerite in contact with melt (Figs 5a and 5b). These galena are more enriched in Zn (0.84–2.45 wt.%), Cu (0.31–2.30 wt.%), Fe (0.07–0.68 wt.%) and Sb (1.02–2.62 wt.%), compared to the unmelted residual galena.

The four experimental runs G55–G58 at 500°C have bulk compositions corresponding to that of the runs G51–G54 at 600°C. Minor melting is observed in all. The composition of these melts could not be determined due to their insufficient quantity. Sphalerite, galena and Zn-bearing cubanite are common to all the run products except G56, in which galena is absent. Meneghinite ($Pb_{13}CuSb_7S_{24}$) is stable in G55 whereas As-bearing geocronite [$Pb_{14}(Sb,As)_6S_{23}$] and tetrahedrite–tennantite solid solution (Ttr–Tnt_{ss} or 'fahlore') are stable in the other three runs (G56–G58). Relatively larger grains of Zn-bearing cubanite, containing inclusions of a mixture of minute Fe–As-rich and Pb-rich quench crystals are observed in the run products of G55 and G57, whereas small globular Zn-bearing cubanite occurs within Ttr–Tnt_{ss} in G56 and G58. Vermicular intergrowth of galena with Ttr–Tnt_{ss} is observed in G58 (Fig. 5c). Unlike the equilibrium galena phase ($Pb_{48.40}Cu_{0.59}Zn_{0.66}Sb_{0.61}Fe_{0.03}As_{0.01}$ $S_{49.70}$), galena in the intergrowth is variably enriched in Cu (0.41–3.06 wt.%), Zn (0.66–2.49 wt.%), Sb (0.45–1.50 wt.%), Fe (0.05–0.19 wt.%) and As (0.02–0.26 wt.%). In G56, Ttr–Tnt_{ss} can contain minor inclusions of quenched melt (Fig. 5d). The Ttr–Tnt_{ss} phases in G56, G57 and G58 correspond to the structural formulae $Cu_6[Cu_{3.95}(Fe_{1.55}Zn_{0.99}Pb_{0.00})_{\Sigma 2.54}](As_{2.30}Sb_{1.87})_{\Sigma 4.17}S_{13}$, $Cu_6[Cu_{3.35}(Fe_{1.36}Zn_{0.80}Pb_{0.01})_{\Sigma 2.17}](As_{2.23}Sb_{1.75})_{\Sigma 3.98}S_{13}$ and $Cu_6[Cu_{3.54}(Fe_{0.87}Zn_{1.27}Pb_{0.01})_{\Sigma 2.15}](As_{2.17}Sb_{1.84})_{\Sigma 4.01}S_{13}$, respectively.

Discussion

The results of the melting experiments in the system ZnS–PbS–FeS–Cu_2S–Sb_2S_3–As_2S_3 suggest that partial melting may take place in sulfide ore bodies close to 500°C. Melting at 500°C is observed in experimental runs in which both Sb and As are present, though not in those in which only Sb is present. This temperature is much lower than the reported minimum temperature of melting of 593 ± 2°C in the system ZnS–PbS–FeS–Cu_2S–S by Pruseth *et al.* (2014). The presence of Sb and As appears to lower significantly the solidus temperature in the system ZnS–PbS–FeS–Cu_2S. Regardless of the fact that low-melting chalcophile elements (LMCEs) promote melting and are generally enriched in the sulfide partial melt (Frost *et al.*, 2002), it is observed in our experiments at 600°C that only a small amount of an Sb-rich melt is produced when Pb is absent (e.g. G9). Considerable amounts of melt are obtained in all experiments containing PbS, which indicates the important role of PbS in producing sulfide partial melts. Note, however, that the presence of PbS only does not ensure partial melting of an assemblage of sulfide minerals. As shown by Pruseth *et al.* (2014), melt might be produced if PbS is accompanied by Cu and S in excess of a monosulfidic proportion. In the absence of PbS, Cu could contribute towards the stabilisation of tetrahedrite and cubanite and no substantial melting would occur, as is evident from the PbS-free run G9, in which only a very minor amount of melt is associated with an assemblage consisting of tetrahedrite, Zn-bearing cubanite, sphalerite and native Sb. Although, the starting bulk compositions are monosulfidic in nature, the melts obtained are S-deficient over Σmetals and are relatively enriched in Cu, Sb, Pb and As in comparison to Fe and Zn. Non-stoichiometric S enrichment of solid phases such as sphalerite and galena compensate for the S deficiency in the melt. Sphalerite and galena are the restite sulfide

https://doi.org/10.1180/mgm.2020.79 Published online by Cambridge University Press

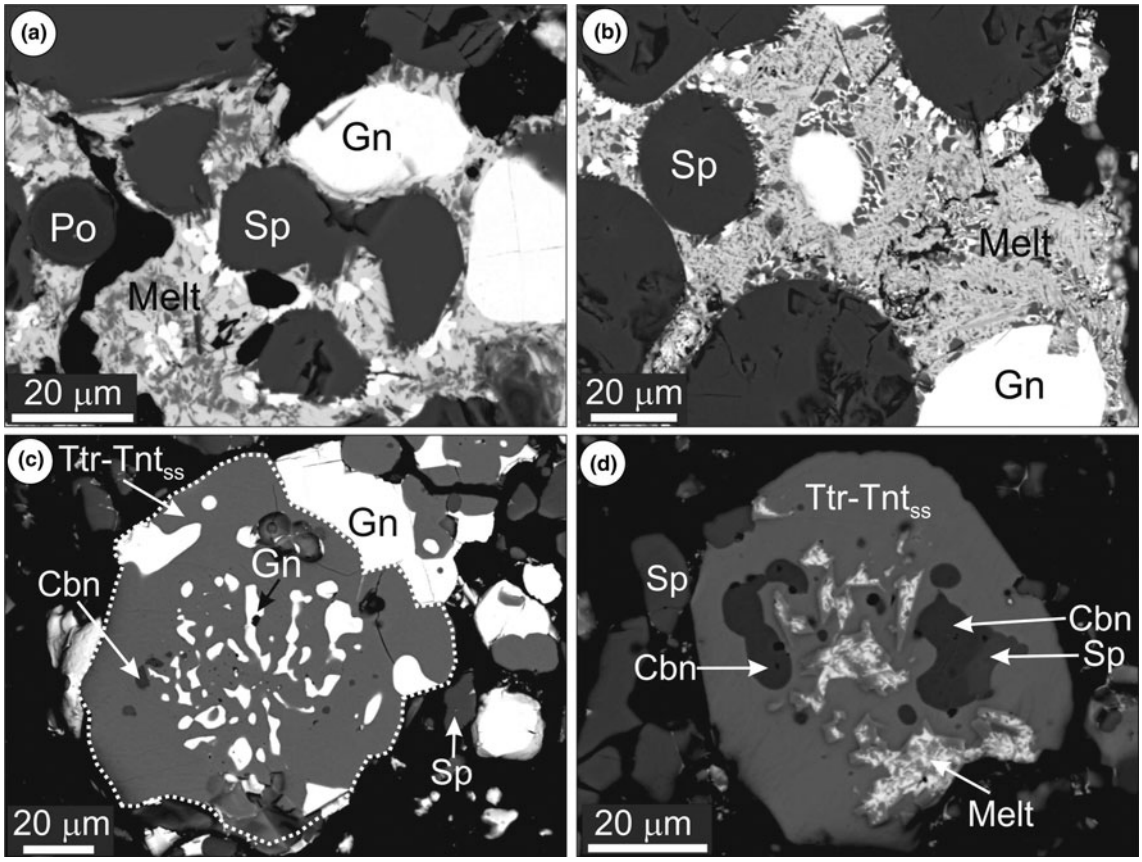

Fig. 5. BSE images of stable phases and quenched melt textures from the runs G51 and G53 (*a* and *b*) at 600°C, the presence of vermicular intergrowth of galena and Ttr–Tnt$_{ss}$ in the run G58 (*c*) and globular cubanite and melt within Ttr–Tnt$_{ss}$ in the run G56 (*d*).

phases in all the experimental run products at both 500 and 600°C except in G9 (PbS-free run), in which galena is absent. Depending upon the bulk run composition, Zn-bearing cubanite appears in some run products both at 500 and 600°C. The Zn-bearing cubanite varies in composition, with 15.45–17.81 wt.% Cu, 36.79–43.41 wt.% Fe and 3.31–8.28 wt.% Zn. Meneghinite, tennantite–tetrahedrite and As-bearing geocronite are the sulfosalt phases encountered at 500°C. None of these phases exist in the run products at 600°C, except in that of G9 in which tetrahedrite is a stable phase. The constituents of the sulfosalts are incorporated in the melts, which are more abundant at 600°C.

Pure tetrahedrite $Cu_6(Cu_4Cu_2)Sb_4S_{12}S$ melts at 573°C (Tatsuka and Morimoto, 1977), whereas pure tennantite $Cu_6(Cu_4Cu_2)As_4S_{12}S$ melts at 665°C (Maske and Skinner, 1971). There is no experimental study on the effect of Zn replacing Cu, however, the incorporation of Fe has been shown to result in an increase of melting temperature of tetrahedrite from 573 to 661°C (Tatsuka and Morimoto, 1977). Thus, the incorporation of both As and Fe results in a higher temperature of melting and therefore, melting of tetrahedrite at a lower temperature cannot be ascribed to the presence of Fe or As in the system. However, as observed in the present investigation, the stability of tetrahedrite also depends on the presence or absence of PbS, as tetrahedrite is observed in none of the PbS-bearing run products at 600°C, but is present in the PbS-free run G9. A Cu_2S-rich melt might exist above 459°C in equilibrium with galena and tetrahedrite, as evidenced from experimental studies in the ternary system PbS–Cu_2S–Sb_2S_3 (Pruseth *et al.*, 1997). Skinnerite ($Cu_{12}Sb_4S_{12}$), which exists in equilibrium with the Cu_2S-rich melt has a composition very similar to that of tetrahedrite [$Cu_6(Cu_4Cu_2)Sb_4S_{12}S$] though with one S less. Skinnerite is a rare mineral and its rarity has been ascribed to the lower S fugacity required for its stabilisation (Pruseth *et al.*, 1997). In fact, any bulk composition with $Cu_2S > Sb_2S_3$ in the system PbS–Cu_2S–Sb_2S_3 is S deficient and explains the stability of skinnerite in this system. Consistent with this argument skinnerite has been shown to have a tendency to break down to tetrahedrite + native Sb (Hoda and Chang, 1975). Thus, it is highly probable that at slightly higher sulfur fugacity, as might be provided by the monosulfidic bulk compositions in the present investigation, tetrahedrite becomes stable in the place of skinnerite. In the 500°C phase diagram of Pruseth *et al.* (1997), galena and skinnerite are almost collinear with the most Sb_2S_3-rich tip E of the Cu_2S-rich melt field (see Fig. 6a), suggesting that a melt of this composition might represent a eutectic between galena and tetrahedrite at higher S fugacity. Thus, textures with inclusions of vermicular galena within tetrahedrite in run G58 (e.g., Fig. 5c) could be due to the simultaneous crystallisation of galena and tetrahedrite from a residual melt that is trapped in early-formed tetrahedrite growing from the same melt. However, the composition of the entire domain containing tetrahedrite and vermicular galena (the dotted area in Fig. 5c) is found to match with the composition of the point E (Fig. 6a), when expressed in terms of mol.% galena and tetrahedrite of equivalent composition. This suggests that no early-formed tetrahedrite existed and the vermicular galena and the tetrahedrite enclosing it simultaneously

https://doi.org/10.1180/mgm.2020.79 Published online by Cambridge University Press

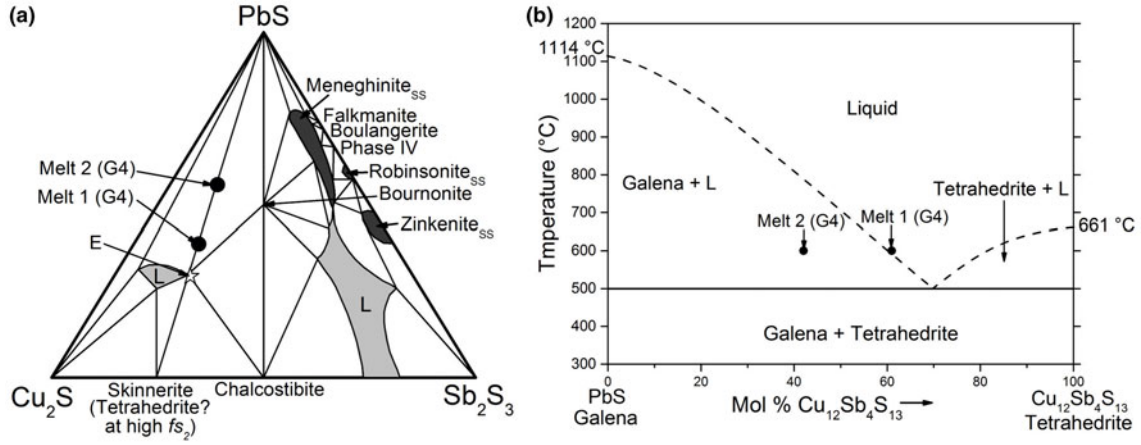

Fig. 6. (*a*) The composition of Melt 1 and Melt 2 (filled circles) of the run G4 projected on the ternary system Cu_2S–PbS–Sb_2S_3 at 500°C (Pruseth *et al.*, 1997). The tetrahedrite:galena ratio of 70:30 mol.% obtained from the dotted area in Fig. 5c coincides with point E, which is collinear with galena and skinnerite. (*b*) Tentative tetrahedrite–galena binary phase diagram at higher f_{S_2}, with proposed eutectic at tetrahedrite:galena = 70:30 mol.% showing Melt 2 is unlikely to be a liquidus phase.

crystallised from melt during the quenching of the experimental run. The composition at point E is 70 mol.% skinnerite and 30 mol.% galena. Thus, a eutectic between galena and pure tetrahedrite could be inferred to exist at ~70 mol.% tetrahedrite and ~500°C. The crystallisation of the vermicular galena from the quenched melt is evidenced by the incorporation of variable amounts of Cu (0.41–3.06 wt.%), Zn (0.66–2.49 wt.%), Sb (0.45–1.50 wt.%), Fe (0.05–0.19 wt.%) and As (0.02–0.26 wt.%). In contrast, the stable solid galena is almost pure PbS ($Pb_{48.40}Cu_{0.59}Zn_{0.66}Sb_{0.61}Fe_{0.03}As_{0.01}S_{49.70}$), with negligible impurities (see Table 2). In the absence of galena, such as in run G56, in which the Fe content is high, As-bearing geocronite is stable with, most probably, a different composition of the Cu_2S-rich melt, which gives rise to an intergrowth of tetrahedrite, cubanite, sphalerite and aggregates of fine crystals with the average composition of 20.44 wt.% S, 4.33 wt.% Fe, 12.26 wt.% As, 8.86 wt.% Cu, 1.45 wt.% Zn, 15. 42 wt.% Sb and 37.80 wt.% Pb (Fig. 5d). Note that very small amounts of cubanite and sphalerite are also present in the tetrahedrite–galena intergrowth in G58 (Fig. 5c).

Galena–tetrahedrite intergrowths, with a higher proportion of galena than can be explained by a eutectic at tetrahedrite: galena = 70:30 mol.%, are also encountered in natural ore deposits, e.g. the one from Bleikvassli (Fig. 3e of Cook *et al.*, 1998) (Norway). Similar intergrowths, formed at 600°C in the experimental run G4 from Melt 2 (with tetrahedrite:galena ≈ 42:58 by mol.%) (Fig. 3b), is accompanied by a melt in which tetrahedrite:galena ≈ 61:39 by mol.% (Melt 1). Both these melts plot on the line joining galena and skinnerite in Fig. 6a. The possibility is that the two melts represent two immiscible liquids in the present experimental system or they separated from a single melt during quenching of the experiment. The latter appears more appropriate as the composition of Melt 2 is unlikely to plot on a liquidus between galena and tetrahedrite (see Fig. 6b). In Pb–Zn ore deposits such as of Rajpura-Dariba and Bleikvassli the bulk ore composition is not likely to plot on the Cu_2S-rich half of the ternary system Cu_2S–PbS–Sb_2S_3. Thus the generation of galena–tetrahedrite intergrowth from a melt appears unlikely in these deposits. However, it has been shown experimentally that the sulfide partial melts are preferably enriched in Cu at 600°C (Pruseth *et al.*, 2014, 2016), which is also the case in this study with the observation that Sb and also As, together with Cu are enriched preferably in the melt. Bournonite, which is a stable phase in the ternary system Cu_2S–PbS–Sb_2S_3, is not obtained in the present experiments, probably due to the presence of Fe and Zn. This probably permits the presence of the Cu_2S-rich melt as a stable phase even when the bulk compositions of the experimental runs do not plot on the Cu_2S-rich half of the system Cu_2S–PbS–Sb_2S_3. Though the presence of Fe stabilises cubanite and meneghinite in the place of bournonite (e.g. G11, G13, G55), the presence of Zn results in the stabilisation of tetrahedrite (e.g. G10, G56–G58). Galena–tetrahedrite intergrowth at 500°C is obtained only when As is present (G58). In such runs, the formation of a Cu_2S-rich melt could have been possible by the stabilisation of As-bearing geocronite in the place of meneghinite, resulting in the enrichment of the rest of the bulk with Cu.

Conclusions

Galena–tetrahedrite intergrowth textures might result by co-crystallisation of galena and tetrahedrite from a sulfide partial melt produced at a minimum temperature of ~500°C during metamorphism of a sulfide ore deposit of suitable bulk composition. Eutectic relation between galena and tetrahedrite at galena:tetrahedrite ≈ 30:70 mol.% at ~500°C are indicated in the system ZnS–FeS–PbS–Cu_2S–Sb_2S_3–As_2S_3, in which the intergrowth produced consists of tetrahedrite–tennantite solid solution and galena. A composition of Cu_2S-rich melt collinear with skinnerite and galena in the ternary system Cu_2S–PbS–Sb_2S_3 (Pruseth *et al.*, 1997) probably represents the eutectic between galena and pure tetrahedrite, which coincidentally happens to be at galena: skinnerite ≈ 30:70 mol.% and ~500°C. It is possible that in monosulfidic bulk compositions, or in natural sulfide ore deposits, tetrahedrite [$Cu_6(Cu_4Cu_2)Sb_4S_{12}S$] rather than skinnerite ($Cu_{12}Sb_4S_{12}$) is the stable equilibrium phase. The possibility of formation of galena–tetrahedrite intergrowths from sulfide melt could be used as an indicator of sulfide partial melting, especially in metamorphosed sulfide ore deposits.

Acknowledgements. BG thanks the Council of Scientific and Industrial Research (CSIR), New Delhi, India, for financial assistance in the form of a Research Fellowship. The experimental work was done using the facility supported by the project EMR/2017/001528 to KLP from SERB, New Delhi.

https://doi.org/10.1180/mgm.2020.79 Published online by Cambridge University Press

SEM-BSE imaging and EPMA data were generated by the equipment procured through a DST funding (IR/S4/ESF-08/2005) to the Department of Geology and Geophysics, IIT Kharagpur. The authors thank three anonymous reviewers and Associate Editor Prof M. Arima for their valuable comments that helped to improve substantially the original manuscript.

References

Anderson A.L. (1934) Some pseudo-eutectic ore textures. *Economic Geology*, **29**, 577–589.

Basu K., Bortnikov N.S., Mishra B., Mookherjee A., Mozgova N.N. and Tzepin A.I. (1984) Significance of transformation textures in fahlores from Rajpura-Dariba polymetallic deposit, Rajasthan, India. *Neues Jahrbuch für Mineralogie Abhandlungen*, **149**, 143–161.

Biagioni C., George L.L., Cook N.J., Makovicky E., Moëlo Y., Pasero M., Sejkora J., Stanley C.J., Welch M.D. and Bosi F. (2020) The tetrahedrite group: Nomenclature and classification. *American Mineralogist*, **105**, 109–122.

Brueckner S.M., Piercey S.J., Pilote J.L., Layne G.D. and Sylvester P.J. (2016) Mineralogy and mineral chemistry of the metamorphosed and precious metal-bearing Ming deposit, Canada. *Ore Geology Reviews*, **72**, 914–939.

Cabri L.J., Hall S.R., Szymanski J.T. and Stewart J.M. (1973) On the transformation of cubanite. *The Canadian Mineralogist*, **12**, 33–38.

Cook N.J. (1996) Mineralogy of the sulphide deposits at Sulitjelma, northern Norway. *Ore Geology Reviews*, **11**, 303–338.

Cook N.J., Spry P.G. and Vokes F.M. (1998) Mineralogy and textural relationships among sulphosalts and related minerals in the Bleikvassli Zn-Pb-(Cu) deposit, Nordland, Norway. *Mineralium Deposita*, **34**, 35–56.

Cook N.J., Ciobanu C.L., Danyushevsky L.V. and Gilbert S. (2011) Minor and trace elements in bornite and associated Cu–(Fe)-sulfides. A LA-ICP-MS study. *Geochimica et Cosmochimica Acta*, **75**, 6473–6496.

Fleet M.E. (1970) Refinement of the crystal structure of cubanite and polymorphism of $CuFe_2S_3$. *Zeitschrift für Kristallografie*, **132**, 276–287.

Frost B.R., Swapp S.M. and Mavrogenes J.A. (2011) Textural evidence for extensive melting of the Broken Hill ore body. *Economic Geology*, **106**, 869–882.

Frost B.R., Mavrogenes J.A. and Tomkins A.G. (2002) Partial melting of sulfide ore deposits during medium- and high-grade metamorphism. *The Canadian Mineralogist*, **40**, 1–18.

Frost B.R., Swapp S.M. and Gregory R.W. (2005) Prolonged existence of sulfide melt in the Broken Hill orebody, New South Wales, Australia. *The Canadian Mineralogist*, **43**, 479–493.

Gemmell J.B., Zantop H. and Birnie R.W. (1989) Silver sulfosalts of the Santo Niño vein, Fresnillo District, Zacatecas, Mexico. *The Canadian Mineralogist*, **27**, 401–418.

Govinda Rao B., Parihar R., Pruseth K.L. and Mishra B. (2017) The occurrence of breithauptite and nisbite-like Sb-Ni phases at Sindesar-Khurd, Rajasthan, India: implications for melt assisted sulfide remobilization. *The Canadian Mineralogist*, **55**, 75–87.

Govindarao B., Pruseth K.L. and Mishra B. (2018) Sulfide partial melting and chalcopyrite disease: An experimental study. *American Mineralogist*, **103**, 1200–1207.

Hoda S.N. and Chang L.L.Y. (1975) Phase relations in the pseudo-ternary system PbS–Cu_2S–Sb_2S_3 and the synthesis of meneghinite. *The Canadian Mineralogist*, **13**, 388–393.

Kojima S. and Sugaki A. (1984) Phase relations in the central portion of the Cu–Fe–Zn–S system between 800° and 500°C. *Mineralogical Journal*, **12**, 15–28.

Kouzmanov K. (2004) Galena-bearing myrmekitic intergrowths from the Radka deposit, Bulgaria: Origin and mechanisms of formation. *Geochemistry, Mineralogy and Petrology*, **41**, 17–30.

Lindgren W. (1930) Pseudo-eutectic textures. *Economic Geology*, **25**, 1–13.

Maske S. and Skinner B.J. (1971) Studies of the sulfosalts of copper. I. Phases and phase relations in the system Cu–As–S. *Economic Geology*, **66**, 901–918.

Matt P., Powell W., deLorraine W.F. and Chiarenzelli J. (2019) Sulfide and silicate anatexis in the Balmat zinc deposit (New York, USA) and its implications for ore remobilization. *Ore Geology Reviews*, **107**, 392–401.

Mavrogenes J.A., MacIntosh W.I. and Ellis D. (2001) Partial melting of the Broken Hill galena-sphalerite ore: experimental studies in the system PbS-FeS-ZnS-(Ag_2S). *Economic Geology*, **96**, 205–210.

Mavrogenes J.A., Frost R. and Sparks H.A. (2013) Experimental evidence of sulfide melt evolution via immiscibility and fractional crystallization. *The Canadian Mineralogist*, **51**, 841–850.

Mishra B. and Bernhardt H.-J. (2009) Metamorphism, graphite crystallinity and sulfide anatexis of the Rampura-Agucha massive sulfide deposit, northwestern India. *Mineralium Deposita*, **44**, 183–204.

Pruseth K.L., Mishra B. and Bernhardt H.-J. (1997) Phase relations in the Cu_2S-PbS-Sb_2S_3 system: an experimental appraisal and application to natural polymetallic sulfide ores. *Economic Geology*, **92**, 720–732.

Pruseth K.L., Jehan N., Sahu P. and Mishra B. (2014) The possibility of a ZnS-bearing sulfide melt at 600°C: Evidence from the Rajpura–Dariba deposit, India, supported by laboratory melting experiment. *Ore Geology Reviews*, **60**, 50–59.

Pruseth K.L., Mishra B., Jehan N. and Kumar B. (2016) Evidence of sulfide melting and melt fractionation during amphibolite facies metamorphism of the Rajpura-Dariba polymetallic sulfide ores. *Ore Geology Reviews*, **72**, 1213–1223.

Putnis A. (1977) Electron microscope study of phase transformation in cubanite. *Physics and Chemistry of Minerals*, **1**, 335–349.

Ramdohr P. (1969) *The Ore Minerals and Their Intergrowths*. 3rd edn. Pergamon, Oxford, UK.

Schwartz G.M. (1939) Significance of bornite-chalcocite microtexture. *Economic Geology*, **34**, 399–418.

Schwartz G.M. and Park C.F. (1932) A microscopic study of ores from the Campbell Mine, Bisbee, Arizona. *Economic Geology*, **27**, 39–51.

Scott S.D. (1974) Experimental methods in sulfide synthesis. Pp. S1–S38 in: *Sulfide Mineralogy* (P.H. Ribbe, editor). Reviews in Mineralogy, Vol. 1. Mineralogical Association of America, Washington, DC.

Sparks H.A. and Mavrogenes J.A. (2005) Sulfide melt inclusions as evidence for the existence of a sulfide partial melt at Broken Hill, Australia. *Economic Geology*, **100**, 773–779.

Szymanski J.T. (1974) The crystal structure of high temperature $CuFe_2S_3$. *Zeitschrift für Kristallografie*, **140**, 240–248.

Tatsuka K. and Morimoto N. (1977) Tetrahedrite stability relation in the Cu-Fe-Sb-S system. *American Mineralogist*, **62**, 1101–1109.

Tomkins A.G. and Mavrogenes J.A. (2002) Mobilization of gold as a polymetallic melt during pelite anatexis at the Challenger deposit, South Australia: a metamorphosed Archean gold deposit. *Economic Geology*, **97**, 1249–1271.

Tomkins A.G. and Mavrogenes J.A. (2003) Generation of metal-rich felsic magmas during crustal anatexis. *Geology*, **31**, 765–768.

Tomkins A.G., Pattison D.R.M. and Frost B.R. (2007) On the initiation of metamorphic sulfide anatexis. *Journal of Petrology*, **48**, 511–535.

Whitney D.L. and Evans B.W. (2010) Abbreviations for names of rock-forming minerals. *American Mineralogist*, **195**, 185–187.

https://doi.org/10.1180/mgm.2020.79 Published online by Cambridge University Press